An Acad Bras Cienc (2023) 95(Suppl. 3): e20220821 DOI 10.1590/0001-3765202320220821
Anais da Academia Brasileira de Ciências | *Annals of the Brazilian Academy of Sciences*
Printed ISSN 0001-3765 I Online ISSN 1678-2690
www.scielo.br/aabc | www.fb.com/aabcjournal

GEOSCIENCES

Glaciological Mass balance of Znosko Glacier, King George Island

WILSON SUAREZ, CINTHYA BELLO, ROLANDO CRUZ, JUAN ZEGARRA, SANDRO ARIAS & FABIAN BRONDI

Abstract: The present article objective is to determine the net mass balance of the glacier Znosko for periods 2018-2019 and 2019-2020. It is situated on King George Island which belongs to the groups Shetland of the South, Antarctic Peninsula region. For this objective, during February 2018 a net of 19 stakes (which were controlled once during February 2019 and 2020) were installed on the glacier ablation zone, drilling in the accumulation zone and about flights using unmanned aerial vehicles (UAV) to control the glacier zone and geomorphological changes. For the year 2020, it was determined a glacier area of 1.71 ± 0.02 km^2, moreover, using five different methods of interpolation, it was obtained on average, as a result, a specific net balance of -590.7 ± 46.6 mm w.e (in water equivalent) for 2018-2019 and -686.7 ± 28.2 mm w.e for 2019-2020, being the ELA altitude 146.5 ± 18.2 m and 144.2 ± 8.3 m respectively. The two consecutive years represent negative net mass balances which are in accordance with other similar studies on this region, also glacier data were obtained on a zone that is characterized by its difficult access.

Key words: Antarctic, King George Island, Admiralty Bay, Mass balance, Znosko Glacier.

INTRODUCTION

Glacier studies began in 1894 with the creation of the International Glacier Commission whose work was later assumed by the World Glacier Monitoring Service (WGMS). The WGMS is today co-responsible for the Global Terrestrial Network for Glaciers and the Global Land Ice Measurement from Space (GLIMS) project in charge of the global inventory of glacier mass balance, volume, and fluctuation data based on field and remote sensing measurements (Allison et al. 2019, Silva et al. 2020). The glacier mass balance is generally determined using glaciological (direct) and geodetic (indirect) methods. The glaciological method determines surface (annual) mass balance by installing a stake network in the ablation zone and digging snow pits in the accumulation zone. This method is generally applied in small and safely accessible glaciers. On the other hand, the geodetic method calculates the volume change in large and remote glaciers by using two or more topographic data sets at different multi-annual time scales (Fischer 2010). Most glaciers worldwide are sensitive to climate change; they either advance or retreat in response to changes in precipitation, temperature, and other variables.

The Randolph Glacier Inventory version 6 (RGI Consortium 2017) estimates the number of Antarctic and sub-Antarctic glaciers (2752) covering an area of 132,867 ± 6,643 km^2, excluding the ice sheet. The Antarctic Peninsula has recorded significant warming since the

mid-20th century (Siegert et al. 2019). The impacts of change on various components of the cryosphere have resulted in a) the rise of sea level (Bamber et al. 2018), b) the collapse of ice shelves (Rott et al. 2011, Berthier et al. 2012, Cook et al. 2014,), c) variations in the sea ice extent and seasonality, d) acceleration of glacial retreat, e) changes in snowline altitude (Arigony-Neto et al. 2009), f) increase in freshwater discharge into the ocean (Falk et al. 2018), g) increase in ice-free areas, h) changes in glacial morphology. However, there is evidence that the northern part of the Antarctic Peninsula has experienced a cooling effect in the last two decades (Carrasco 2013, Oliva et al. 2016, Turner et al. 2016, Bello et al. 2022), resulting in glacial retreat deceleration and positive mass balances in some glaciers in the South Shetland Islands. Using satellite images (1956–2018), Da Rosa et al. (2020) observed a decrease in the retreat rate of Ecology, Sphinx, Baranowski, Tower and Windy glaciers (Warszawa Ice Field) from 2000 to 2018. This observation contrasts with that observed in the period 1979–2000, demonstrating that glaciers with small areas respond to changes in annual air temperature on a decadal scale. (Pętlicki et al. 2017) reported that the rate of change in elevation of the Ecology Glacier front decreased between the analyzed periods (1979–2001 and, 2012–2016), being more In the latter. In addition, the Ecology and Sphinx glacier system lost 41% of its area from 1979–2012, indicating a negative mass balance (Sobota et al. 2015) however, it a mean mass balance of +17.8 cm w.e. for 2012-2013. Simões et al. (2015) reported that Wanda Glacier lost 0.71 km^2 of its area (1979–2011). The WGMS database has records exceeding 15 years of continuous measurements of surface mass balances (glaciological method) for only two glaciers in the region (Hurd and Johnsons glaciers) in the South Shetland Islands. The surface mass balance of Hurd and Johnsons glaciers was estimated to be 0.15 ± 0.10 m w.e. and −0.09 ± 0.17 m w.e., respectively for 2002–2011 (Navarro et al. 2013). This observation confirmed a reduction in the mass loss of these glaciers during the observed 1957–2000 period that can be attributed to a series of factors (Antarctic circumpolar current changes, reduced melting, and low summer temperatures).

The Collins Glacier (also known as the Bellingshausen Ice Dome) in King George Island has a record of mass balance for four (4) years (2008–2011), with a total mass loss of −0.31 ± 0.76 m w.e. It registered positive mass balances 2010 (0.37 ± 0.76 m w.e.) and 2011 (0.09 ± 0.76 m w.e.) (Mavlyudov 2014) In addition, Simões et al. (2004) analyzed four (4) small glaciers in the Keller Peninsula (Admiralty Bay), determining that they have lost between 44% and 83% of their surface from 1979 to 2000. Bello et al. (2020) combined Ground Penetrating Radar (GPR) data and digital images from Unmanned Aerial Vehicles (UAV) to create an ice thickness base map of the Znosko glacier (ZG). They also calculated a geodetic mass balance for the same area for 2012–2020 using UAV surveys, obtaining a negative mass balance of -18 m w.e. (Bello et al. 2023).

Considering the different results observed in this region, the main objective of the present study is to estimate the net mass balance of ZG using the glaciological method for two years (2019 and 2020).

MATERIALS AND METHODS

Study area

King George Island (KGI) is the largest island of the South Shetland archipelago spanning an area of 1250 km^2, located about 100 km from the Antarctic Peninsula (Lagger et al. 2018). It is a glacial basin (marine or land-terminating) of ice covering about 90% of the island (Simões et al.

1999). This ice cap has a maximum height of 720 m above sea level (a.s.l.) (central part) (Rückamp et al. 2010). It is sensitive to variations in climate due to the maritime climatic condition (Ferron et al. 2004, Rückamp et al. 2010, Rückamp & Blindow 2012). The snow line varies from 140 m to 210 m a.s.l. (Birkenmajer 2002). The mean annual precipitation on the Bellingshausen station in Maxwell Bay was 701.3 mm from 1968 to 2011 (Kejna et al. 2013). The mean air temperature was −2.8 °C (1947–1995) on the Fildes Peninsula (Simões et al.1999) and −2.5 °C (1948–2011) on KGI (Kejna et al. 2013). ZG is located in the KGI, to the west of Admiralty Bay (Mackellar Inlet) and adjacent to the Peruvian Machu Picchu Scientific Station (ECAMP) (62°05.5'S and 58°28.5'W). In 2013, the National Service of Meteorology and Hydrology of Peru (SENAMHI) and the National Water Authority (ANA) participated in the 22nd Peruvian Scientific Expedition to Antarctica (ANTAR XXII) to examine the ZG and confirm whether the glacier met the technical and safety conditions for the evaluation of its mass balance. A network of stakes was installed (19) on the ZG during the 25th expedition (2018), which was monitored during ANTAR XXVI (2019) and XXVII (2020).

Data

Meteorological data

This study used the monthly precipitation and surface air temperature data from March 2015 to February 2021 from the Russian Bellingshausen Scientific station (62.20°S, 58.97°W), on 16 m a.s.l. (Figure 1). The precipitation data was downloaded from https://www.ncdc.noaa.gov/cdo-web/ of the National Centers for Environmental Information of the National Oceanic and Atmospheric Administration (USA). The surface air temperature data were obtained from the Met Reader database (https://legacy.bas.ac.uk/met/READER/surface/Bellingshausen.All.temperature.txt), which the British Antarctic Survey manages.

Ice cores and ablation stakes

Shallow snow and ice cores zone were obtained from the accumulation in the Austral summers from 2018 to 2020 (4 in 2018, 3 in 2019, and 4 in 2020). Nineteen stakes were installed in the ablation zone in 2018 (see Figure 2) to determine the annual ablation. Nevertheless, only seven were found in January 2019 due to the thick snow cover and 15 stakes in February 2020. The length of the stakes (10 m) allowed them to be used for measurements in all years of the study. Field visits were made during the last week of January to the first week of February (once every year) during the study period (2019 and 2020) at the end of the summer season.

Table I shows the position of the stakes installed in the year 2018.

Satellite Images and Orthophotos

The Antarctic Peninsula region and its surroundings are characterized by a significant cloud cover throughout the year, allowing only short periods during the summer months to obtain an adequate image. We used passive satellite images and orthophotos obtained using a UAV to measure glacier area and determine the snow line altitude. The first image corresponds to a WorldView-2 type Peru's Ministry of Foreign Affairs provided. In addition, a Landsat 8 image of 2018 and Sentinel-2 of 2019 were downloaded from the Glovis portal from the United States Geological Service. The orthophotos were generated using a UAV Phantom 4 Pro with a rotary wing (quadcopter) capable of withstanding winds up to 20 knots. It included an RGB camera (resolution of 20 megapixels and field of view 84°), and the images were processed with the Pix 4D software. The orthophotos were also used

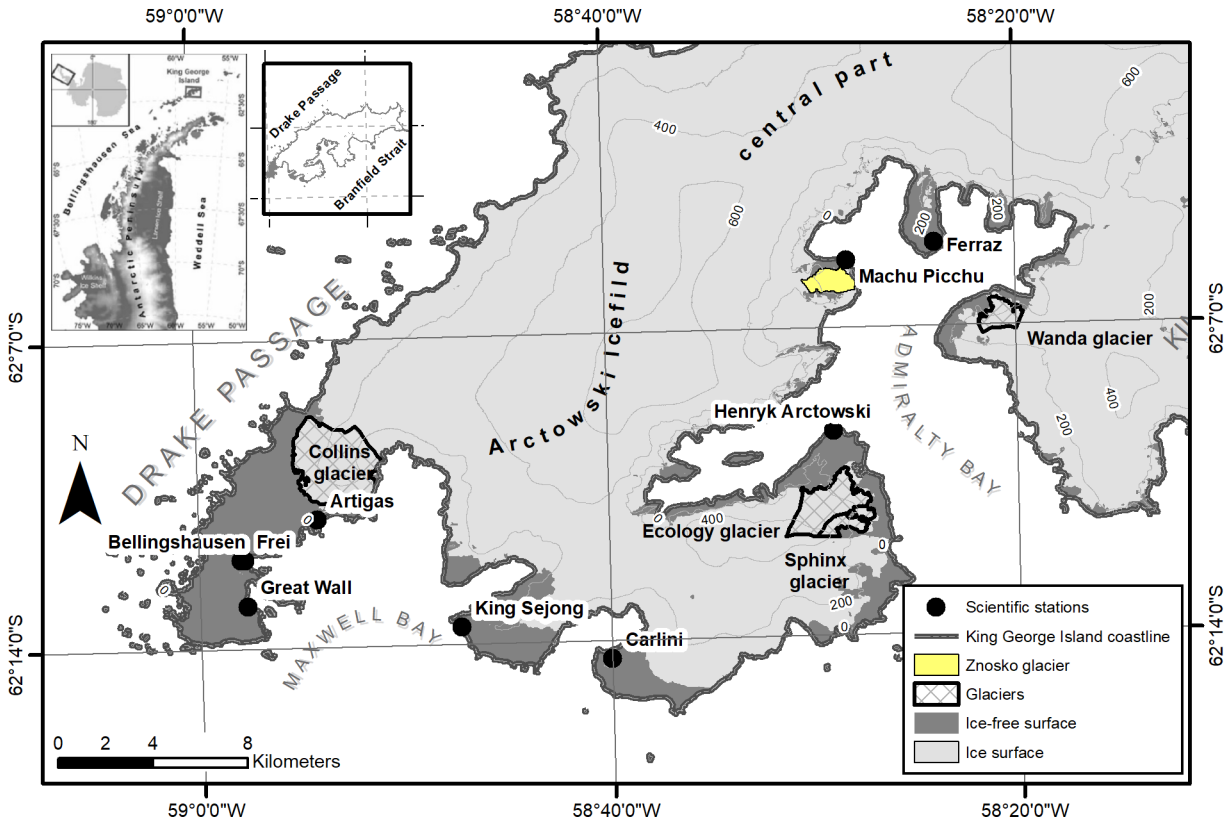

Figure 1. Location map of the Znosko Glacier and nearby scientific stations.

to generate two digital elevation models for 2019 and 2020 at sub-meter resolution (0.5 m). A description of the main technical characteristics of the images and orthophotos used, and their role in the present study are presented in Table II.

Methodology

There are different methods to calculate the glacier mass balance, such as glaciological (Paterson 1994), geodetic (Kaser et al. 2003, Hagg et al. 2004), hydrological (Kaser et al. 2003), statistical (Ostrem & Stanley 1966, Lliboutry 1974), methods to determine the equilibrium line altitude (ELA) position (Ostrem & Stanley 1966), and methods to determine the terminal position of the glacier (Paterson 1994). This research work also aimed to provide essential considerations for field campaigns (technical, climatic and logistical aspects) to develop a net mass balance for monitoring glaciers in Antarctica and processing the collected data, in this work, the glaciological method was used.

Field season

Fieldwork in the Antarctica region has a series of limitations and conditions that are different from the other parts of the world, mainly due to glacier extension, inaccessibility, extreme climatic conditions, and high logistical costs. For the study of ZG, ECAMP provides logistical support for ground activities only during Austral summers, mainly January and February each year. Therefore, any installed equipment does not have supervision or control until the following Austral summer. The summer months have the best meteorological conditions for accessing the glaciers. However, these ideal conditions

Table I. Location of stakes installed in 2018.

Name	X	Y	Altitud (m)
Stake_01	423410	3114059	21
Stake_02	423332	3114045	28
Stake_03	423250	3114020	42
Stake_04	423132	3113994	55
Stake_05	423008	3113956	80
Stake_06	422911	3113923	84
Stake_07	422815	3113868	121
Stake_08	422713	3113874	110
Stake_09	422571	3113872	109
Stake_10	422494	3113849	121
Stake_11	422367	3113786	143
Stake_12	422581	3113596	126
Stake_13	422862	3113671	99
Stake_14	423016	3113717	81
Stake_15	423286	3113728	52
Stake_16	423161	3114131	39
Stake_17	422955	3114080	64
Stake_18	422746	3114065	91
Stake_19	422577	3114043	116

Projected coordinate system: WGS 1984 UTM zone 21S.

do not exceed 70% of those foreseen during preparation of scientific expeditions, limiting the work on the glacier. Regarding accessibility, most of the glaciers in KGI are marine-terminating (tidewater) and generally do not allow direct access to the frontal sector. Thus, this requires complementing the monitoring process with remote sensing tools.

The accumulation season coincides with winter and the ablation season coincides with summer in glaciers characterized dominant accumulation during winter (Cogley et al. 2011).

The glaciological method was used based on in situ measurement of accumulation and ablation to calculate the net mass balance for each year. A lightweight and easily portable Kovacs auger was used for accumulation measurements (Figure 4). In the ablation zone, aluminum control stakes were installed at different altitudes of the glacier to measure the superficial mass loss. We established the first network along the main flow line of the glacier and others in parallel. The geographical position of each stake was recorded with the help of a portable GPS. The stakes were assembled by five rods of 2 m each (10 m in total), joined by a pivoting or articulated structure to increase their flexibility and avoid damage in the absence of field visits until the following year (austral summer). These rods were installed at a depth of approximately 9 m. It is essential to correctly identify the ice and snow levels as they are prone to errors. Different authors have described the general methodology for using stakes and accumulation cores since the middle of the last century (Ostrem & Stanley 1966, Ostrem & Brugman 1991, Kaser et al. 2003, Francou & Pouyaud 2004, Cogley et al. 2011, Rivera et al. 2016). However, due to logistics constraints ZG was monitored only during the Austral summers. So, the measurements were as close as to the end of the maximum melting (end of summer).

Laboratory analysis of the fieldwork data

According to Haeberli (2011), glacier mass balance is the sum of all the processes that add mass to a glacier and take remove it. The accumulation or addition of mass generally occurs in the form of snowfall, the distribution of which can be modified by snowdrifts and/or avalanches. The melting of snow and ice is the predominant form of ablation or mass removal. Still, the calving of tidewater glaciers, ice avalanches from steep hanging glaciers, or evacuation of wind-blown snow during cold or dry conditions can be important at the local level. Different authors have handled the same

Table II. Characteristics of images and orthophotos used in the study.

Instrument	Pixel Resolution	Captor Resolution	Date	Objective	Reference
WorldView 2	< 1m	Pancromatic	Mar 2012	snow line position and glacier delimitation	https://www.aerospace-technology.com/projects/worldview-2/
Landsat 8	30 m	OLI 9 Bands	Feb 2018	snow line position	https://landsat.gsfc.nasa.gov/landsat-8/landsat-8-overview
Sentinel 2	10 m	MSI (Band 2 to 4)	Apr 2019	snow line position	https://sentinel.esa.int/web/sentinel/technical-guides/sentinel-2-msi/references
UAV orthophoto	< 1m	RGB	Jan 2019	DEM and glacier delimitation	-
UAV orthophoto	< 1m	RGB	Feb 2020	DEM, snow line position and glacier delimitation	-

type of definition under different approaches, for example:, Kaser et al. (2003) Jansson et al. (2003) and Cogley et al. (2011).

Mathematically, the mass balance of the glacier can be described as (Lliboutry 1964, Paterson 1994, Dyurgerov 2002):

$$\frac{db}{dt} = \rho \frac{dh}{dt} + \int \frac{d\rho}{dt} dz$$

where, ρ denotes the density of ice of thickness h, varying in time t.

A simplification of the above equation of mass balance at any point on the glacier can be given as:

$$b_i = \rho_0 \Delta h + (\rho_2 h_2 - \rho_1 h_1)$$

where, b_i corresponds to the balance at any point of the glacier, and ρ_0 denotes the density of glacier ice in 0.9 $g.cm^{-3}$. The first component of the equation represents the ice balance, and the second component represents porous material (snow and firn) that changes with time. The accumulation cores and stakes placed on the glacier extend the balance to the entire glacier. The basic principle is to weigh the balance measured by the extrapolated area of the samples to the total area of the glacier, according to the expression:

$$B_n = \frac{\left[\sum \left(b_{n1} S_1 + b_{n2} S_2 + \ldots\ldots\ldots + b_{ni} S_i\right)\right]}{S}$$

where, B_n corresponds to the mass balance of the total glacier, and S denotes the glacier surface, b_{n1}, b_{n2}, and b_{ni} are the area-weighted balance sheet of S_i.

Considering the automation of processes using raster formats and geographic information systems, b_n can be considered as the value of a pixel, while S_n denotes the resolution of the pixels.

One of the main sources of error during mass balance calculations is the treatment of the information coming from the ground and its subsequent extrapolation to the whole glacier for the final calculation (Cuffey & Paterson 2010). This last calculation method is the most commonly used to interpolate ground data following local geomorphological patterns and altitude, which strongly depends on the criterion of the specialist. This study, used 05 interpolation methods contained in ArcMap 10.8 software, as presented in Table III.

Table III. interpolation methods used.

Method	Reference
IDW	Mitas & Mitasova (2005)
Kriging	Oliver & Webster (1990)
Natural Neighbor	Sibson (1981)
Spline	Johnston et al. (2001)
Spline with barrier	Smith & Wessel (1990)

RESULTS

The analysis of satellite images and orthophotos of the ZG determined that the 2020 glacier area was 1.71 ± 0.02 km^2, considering part covered and not covered by debris. In comparison, the part of ZG not covered by debris (exposed part) in 2012, 2019, and 2020 were, respectively, 1.65 ± 0.02 km^2, 1.61 ± 0.02 km^2, and 1.60 ± 0.02 km^2. These findings indicate that the glacier lost 0.06 km^2 area in these last eight years. Between 2019 and 2020, the glacier retreated at 0.02 km^2 because of a mass loss of the calving front. Figure 2 shows a gradual growth of the small lake at the front. This figure also shows the hypsometry of the glacier (bands every 30 m), which was constructed based on the 2020 digital elevation models. It shows that changes in the area have occurred only in the lowest 30 meters of altitude. Most of the glacier surface is between in the bands 90 m to 120 m a.s.l. and between 120 m to 150 m a.s.l., with a difference of 4300 m^2. Figure 2 also shows that the glacier area increases in the upper part, between 240 m and 270 m.a.s.l., due to the shape (widening) of the glacier.

Both precipitation and surface air temperature are determining factors in the ablation and mass gain of a glacier. In the ZG, these variables (also the mass balance) were analyzed by considering the beginning of the annual period from March (n) to February (n + 1) because the stakes measurements and accumulation cores were taken once a year, mainly in February. In addition, the air temperature data (based on six years' record) are presented in Table IV the mean temperature was above 0 °C between December and March, and February being the warmest most (1.6 °C). For the remaining months, the mean temperature was below 0 °C, and August was the coldest month (-5.8 °C). The highest total precipitation was recorded in March (84.9 mm), and the lowest was in July (34.3 mm). Figure 3a compares the seasonality of these two variables in different years. Figure 3b shows linear trends for precipitation and temperature variability for the 2015-2021 period, where 2018-2019 registered the highest annual value of accumulated precipitation at 738.3 mm, while 2016–2017 recorded the lowest annual one, 570.9 mm (Figure 3c). For the mean annual air temperature, 2015-2016 was the coldest (-3.19 °C), while 2016–2017 was the warmest (-1.67 °C). In addition, the years 2018–2019 and 2019–2020 recorded temperatures of -1.75 °C and -1.97 °C, respectively. The mean annual air temperature was below the surface melting temperature during all years (-1.8 °C), and the total mean precipitation was 656.6 mm.

To calculate the glacier net mass balance, we first identify the last year's ice layer the shallow cores, (see Figure 4a). The black dots in this figure show the recorded measurements (the deepest represents the last year's ice layer), and the blue dots show the accumulated content in mm w.e. for the previous year's ice layer of each study core. Last year ice layers were found at a depth of less than 160 cm for 2018-2019 and between 160 and 200 cm for 2019–2020, except for core 4, which did not exceed 80 cm depth. A relevant factor to be considered in the sampling area is the deposition of material coming from the lateral mountains of the glacier. This deposition causes significant superficial melting that accelerates the snow metamorphic process, creating high-density layers that can be mistaken as last year's ice layers.

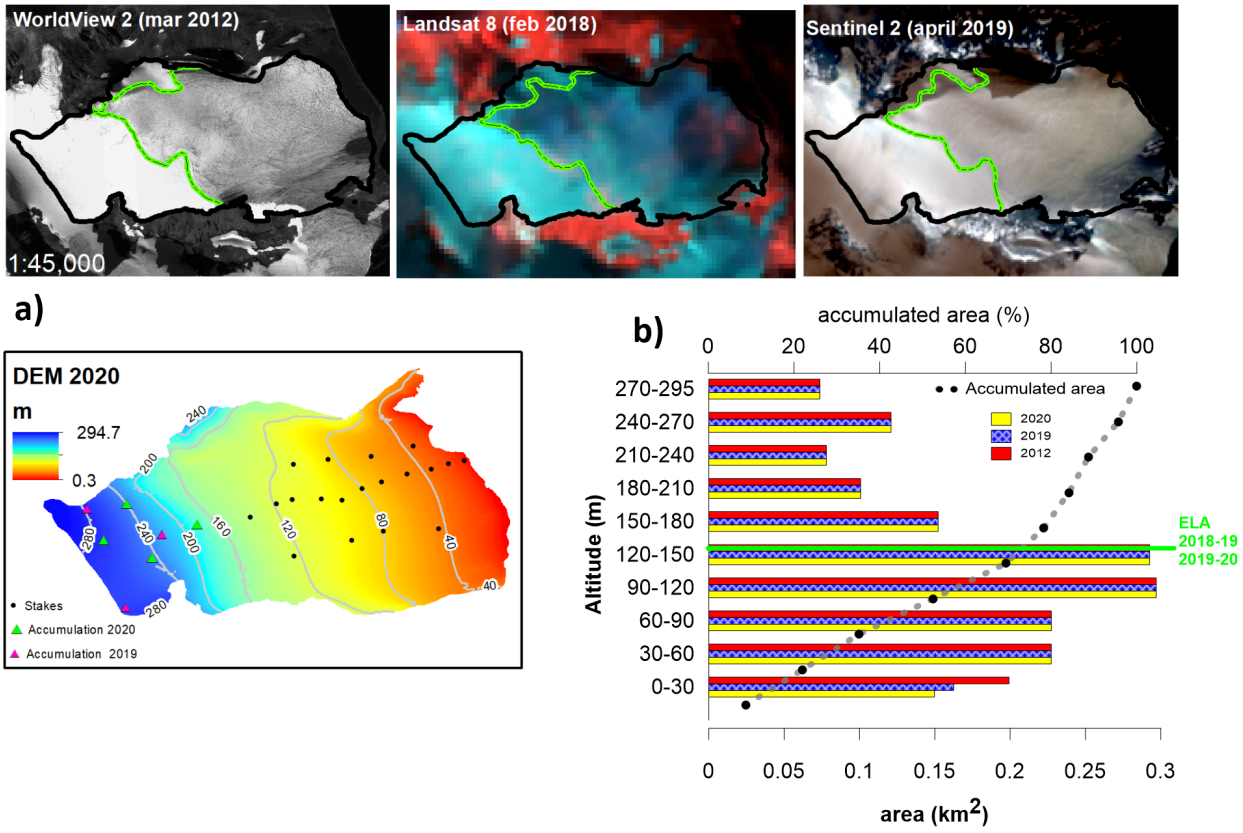

Figure 2. (a) Satellite images used in this study (the green line with black dashes indicates the snow line); (b) hypsometry of the Znosko Glacier for the years 2012, 2019 and 2020.

Concerning the stakes in the ablation zone, of the 19 stakes installed in January 2018, only 7 were located in February 2019 (thick snow layer during fieldwork) and 16 in February 2020 (stake N°1 was lost due to glacier front detachment). Due to insufficient stakes in the 2018–2019 period, it was necessary to reconstitute the missing stakes based on the high linear correlation between (r^2 = 0.925) the stakes of the two study periods. Figure 4b shows the measured stakes (blue dots) and those reconstructed by linear regression (black dots) for 2018–2019. In addition, the independent term of the linear regression of the stakes (observed and reconstituted) shows the position where the net mass balance is zero, i.e., the equilibrium line (158 m a.s.l.). Figure 4b shows a significant correlation (r^2 = 0.66) of the linear regression for the stakes of the 2019–2020 period. The independent term establishes the position of the ELA at 162 m a.s.l. Figure 4c compares all the stakes of the two study periods in ascending order according to their altitude, where stake-07, stake-08, stake-19, and stake-11 show a significant emergence (appearance) unrelated to altitude. For 2018–2019, the highest emergence of the stakes was found around the glacier front, specifically in the environment where ice detachments are observed due to the calving effect. In this case, Stake-01 presented the highest ablation at 2,592 mm w.e, followed by stake-03 at -2,412 mm w.e, with the net ablation recorded at stake-10 at -640 mm w.e. In 2019–2020, the maximum ablation was observed in stake-02 at -3,001 mm w.e., followed by stake-04 at -2,493 mm w.e. The lowest ablation was registered in stake-10 at -776.6 mm w.e.

Table IV. Mean temperature and precipitation for the 2015–2021.

variable	Mar	Apr	May	Jun	Jul	Aug	Sep	Oct	Nov	Dec	Jan	Feb	Annual
T (°C)	0.8	-1.3	-2.5	-4.3	-4.7	-5.8	-4.2	-2.5	-0.9	0.3	1.4	1.6	-1.8
PP (mm)	84.9	55	54.5	53.2	34.3	58.6	56.1	45.3	46	47.7	61.5	59.5	656.6

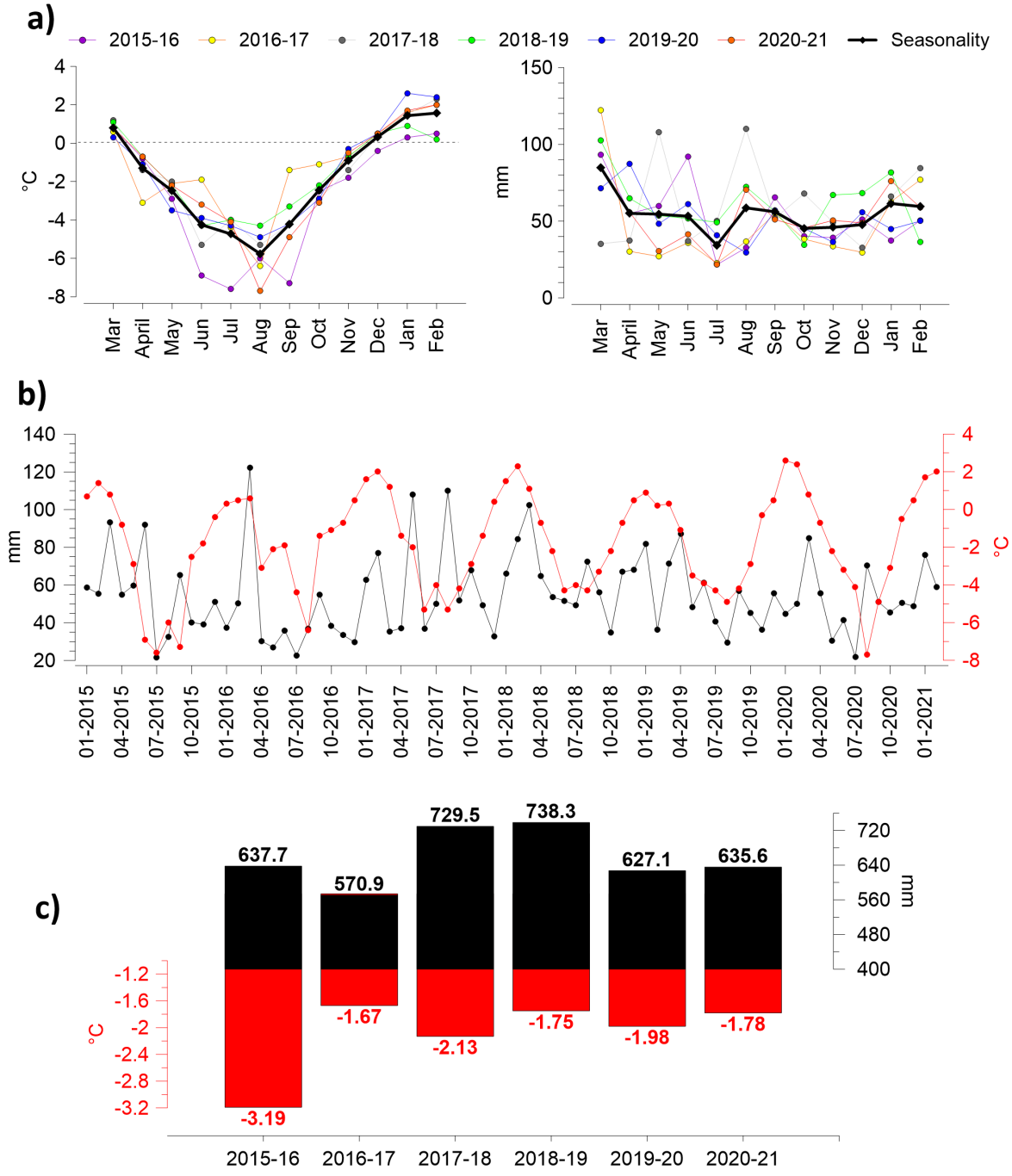

Figure 3. (a) precipitation and air temperature seasonality; (b) series of monthly air temperature and precipitation series (c) comparison between air temperature and precipitation at the sampling year level.

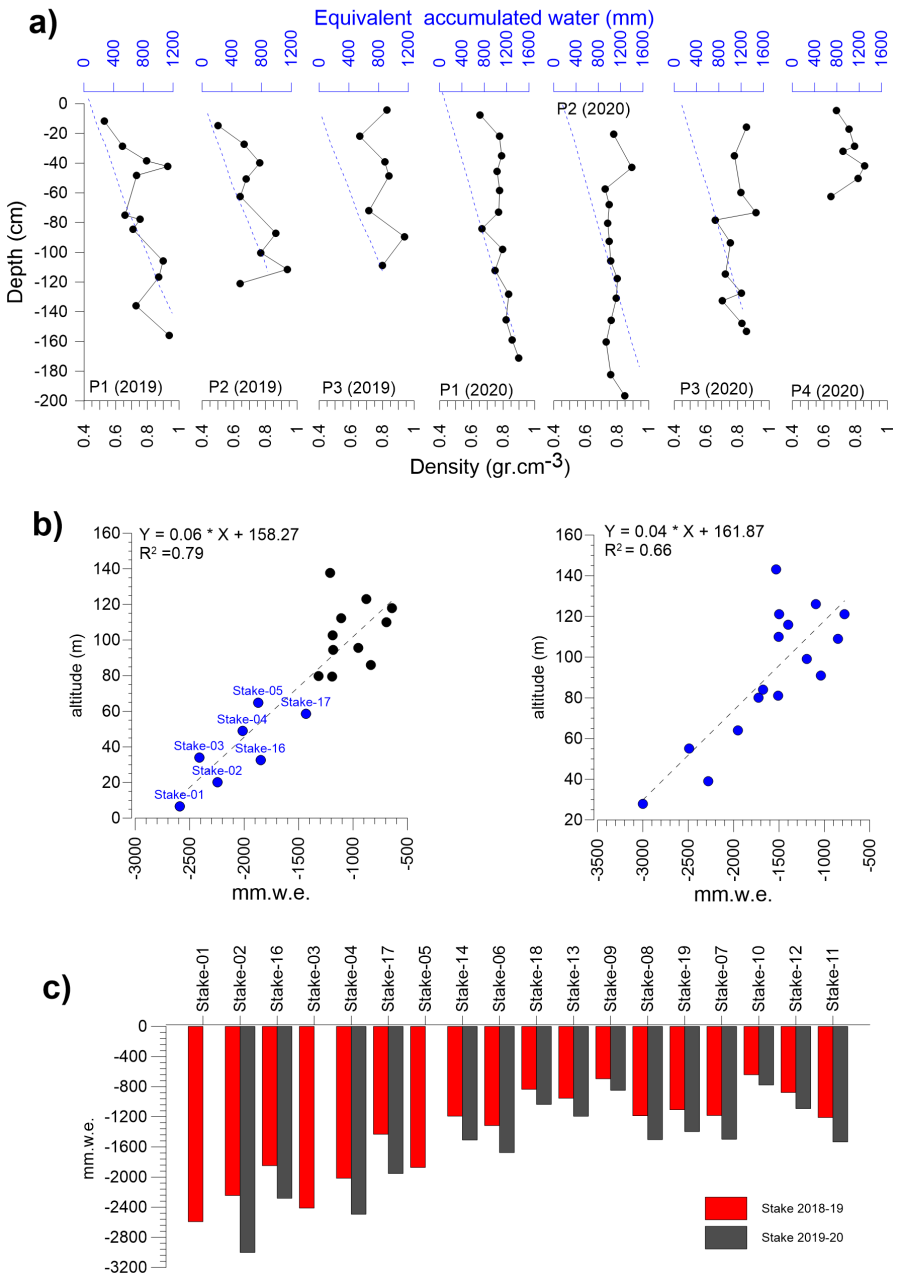

Figure 4. (a) Density profile and equivalent water content for the accumulation area snow cores, (b) on the left: stakes measured for the period from 2018-19, the blue color indicates stakes that were measured directly, and on the right stakes measured for the period from 2019-20 (c) comparison of the emergence of the stakes used in this study.

We used the data from the stakes and shallow cores and the position of the snow line (Figure 2) as a reference for the position of the ELA to determine glacier mass balance for the study periods. Generally, the snow line's position marks the ELA's approximate position at the end of summer. However, it is assumed here that the snow line marks the equilibrium of the snowmelt concerning the air temperature, indirectly marking the beginning of the glacier accumulation zone. Thus, this led to the generation of interpolation support points, assuming a 0.0 mm w.e. value on the snow line. Table V shows the net mass balance for derived from five interpolation methods used for the period 2018–2019, resulting in a mean glacier

net mass balance of -591 ± 47 mm w.e., where the accumulation represents 193 ± 57 mm w.e. with an area of 1.07 ± 0.07 km^2 and the ablation -783 ± 44 mm w.e. with an area of 1.07 ± 0.07 km^2. The most conservative method is the Natural Neighbor with -570 mm w.e., and the IDW method exhibited the most negative net balance with -625 mm w.e. The mean Accumulation Area Ratio (AAR) is 0.34, with the lowest value of 0.3 (IDW) and the highest of 0.36 (Spline). The graphical analysis in Figure 5a shows that the Spline and Spline with barrier methods better represent the shape of the snow line. The average of all methods, the ablation at the front of the glacier is above 2,400 mm w.e., reaching the maximum of -2,622 mm w.e. The accumulation at the top of the glacier is above 900 mm w.e., reaching a maximum of 1,188 mm w.e.

Table VI shows that the mean glacier net mass balance is -687 ± 28 mm w.e. for the period 2019–2020, with an average gain (accumulation) and loss (ablation) of 271 ± 65 mm w.e. (0.55 ± 0.04 km^2) and -958 ± 51 mm w.e. (1.06 ± 0.04 km^2), respectively. The net mass balance calculated by the IDW method presents the lowest value at -707 mm w.e. The most conservative corresponds to the Kriging method with -674 mm w.e. In terms of areas, the Spline method presents the largest accumulation area at 0.58 km^2, and the IDW method shows the smallest area at 0.52 km^2. In the accumulation zone, the IDW method gives the largest area at 1.09 km^2, and Spline has the smallest area at 1.03 km^2. The maximum value of ARR is observed with the Spline method at 0.36 for 2018–2019, and the lowest corresponds to the IDW at 0.32. Figure 5b shows that the Spline and Spline with barrier methods better represents snow line for 2018–2019. Considering the average of all methods, the accumulation is above 1,200 mm w.e., reaching up to 1,550 mm w.e., while there are values above -3,000 mm w.e. in the ablation zone (glacier front), reaching the maximum of -3,130 mm w.e.

Table VII shows the results of ELA analysis for the two study periods, located at a mean altitude of 146.5 ± 9.2 m a.s.l. for the period 2018–2019 (does not consider the staking method), with an elevation interval between 154.4 and 143 m a.s.l. When averaged over the five methods under study, IDW exhibited the highest average position at 154.4 m a.s.l., and Spline displayed the lowest average position at 143 m a.s.l. The stakes method (independent term of the stakes regression equation) showed an altitude of 158.3 m a.s.l.; the highest position recorded for ELA was by the IDW method with 184.9 m a.s.l and the lowest by the Spline method with 106.4 m a.s.l. For 2019–2020, the mean ELA position

Table V. Znosko glacier mass balance for the period 2018-19.

Method	Mass Bilan (mm.w.e.)	Acumulation (mm.w.e.)	Ablation (mm.w.e.)	Acumulation Area (km^2)	Ablation Area (km^2)	AAR
Kriging	-580.6	190.7	-771.3	0.557	1.065	0.34
Spline	-573.5	233.5	-807.0	0.576	1.046	0.36
IDW	-625.3	150.7	-775.9	0.493	1.129	0.30
Natural Neighbor	-570.4	186.2	-756.7	0.560	1.056	0.35
Spline with barrier	-603.5	201.3	-804.7	0.556	1.066	0.34
Mean	-590.7	192.5	-783.1	0.55	1.07	0.34
Error	± 46.6	± 59.6	± 43.9	± 0.06	± 0.07	± 0.05

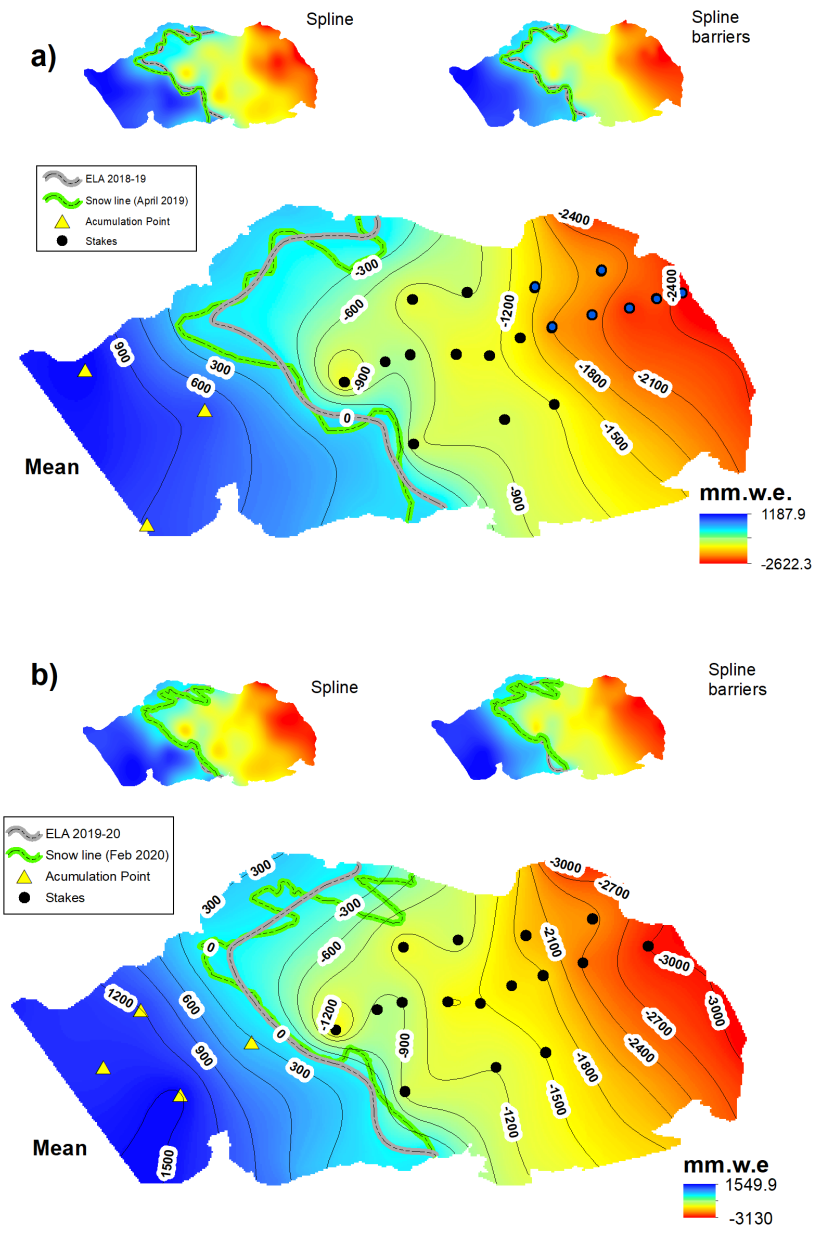

Figure 5. Mass balance for the Znosko Glacier (a) 2018-19 and (b) 2019-20.

based on the five methods was 144.2 ± 8.3 m a.s.l. with an elevation interval between 140.1 to 151.2 m a.s.l. The mean ELA position at 113.2 m a.s.l. determined by the Spline method represents the lowest position and that defined by IDW at 175.2 m a.s.l. represents the lowest. Moreover, according to the stakes regression curve, the ELA is at 161.9 m a.s.l.

CONCLUSIONS AND DISCUSSION

In the Austral summer of 2018 on the ZG, a network of 19 stakes was installed and monitored in parallel with accumulation cores during 2019 and 2020. Accordingly, this glacier's net mass balances were negative (-591 ± 47 mm w.e.,2018–2019) with the ELA at 146.5 ± 9.2 m a.s.l. and -687 ± 28. mm w.e. (2019–2020) with the ELA

Table VI. Znosko glacier mass balance for the period 2019-20.

Method	Mass Bilan (mm.w.e.)	Acumulation (mm.w.e.)	Ablation (mm.w.e.)	Acumulation Area (km^2)	Ablation Area (km^2)	AAR
Kriging	-674.0	274.4	-948.3	0.56	1.05	0.35
Spline	-680.3	320.5	-1000.8	0.58	1.03	0.36
IDW	-707.3	229.5	-936.8	0.52	1.09	0.32
Natural Neighbor	-677.0	265.8	-942.8	0.56	1.05	0.35
Spline with barrier	-695.2	263.0	-959.0	0.56	1.05	0.34
Mean	-686.7	270.7	-957.5	0.55	1.06	0.34
Error	± 28.2	± 65.4	± 51.2	± 0.04	± 0.04	± 0.03

Table VII. ELA position for Znosko Glacier for the periods 2018-19 and 2019-20.

Method	ELA Position to 2018-19 (m)				ELA Position to 2019 - 20 (m)			
	min	Mean	max	Ecart	min	Mean	max	Ecart
Kriging	114.0	145.8	173.5	14.4	127.4	143.1	158.8	9.6
Spline	106.4	143.0	175.0	18.0	113.2	140.1	163.8	12.8
IDW	130.9	154.4	184.9	15.9	130.8	151.2	175.2	11.7
Natural Neighbor	115.4	143.5	170.0	13.2	126.9	143.0	155.9	8.3
Spline with barrier	112.5	145.7	176.2	16.1	124.7	143.6	157.8	9.8
Stakes		158			-	162	-	-
Mean	115.9	146.5	175.9	15.5	124.6	144.2	162.3	10.5
Error	± 18.2	± 9.2	± 11.0	-	± 13.4	± 8.3	± 15.6	-

at 144.2 ± 8.3 m a.s.l. This negative balance is primarily explained by local climatic conditions, where the mean precipitation amounted to 738 mm (2018–2019) and 627 mm (2019–2020). The annual mean air temperature for the last 6 years was above 0 °C between December to March, so glacial melting prevailed. The methodology used for calculating the net mass balance relies on ground samples. Even though we only recovered seven stakes for 2018-2019, it was possible to correlate the existing ones with those of 2019–2020, allowing us to estimate the position of the remaining ones.

Five data interpolation methods were used to calculate the annual mass balance and reduce the source of error, their, mean is the net balance. In addition, the position of the snow line (obtained from satellite images and orthophotos) was used as a visual adjustment element, considering the hypothesis that this is a proxy of the ELA position, albeit a small difference due to the formation of superimposed ice. The five methods of this study can also be used as an indirect method. Spline best represented the shape of the snow line. It is necessary to assume support points on the snow line irrespective of the method used to reduce, interpolation errors. Other determining factors in the loss of glacier mass are as follows: a) material deposition (observed in a zone next to ELA) that accelerates

melting process cannot be ignored, b) the retreat of the glacier front by calving process causes the detachment of ice masses (before the year 2018 was not observed), possibly because the bed of the glacier front is below sea level and the intrusion of water from the sea is undermining the lower part of this glacier (Bello et al. 2020). The observed meteorological data show that, on average, the air temperature was below 0° C and the precipitation in 656 mm, the latter (added to air temperature conditions) allowed a mass gain, but not enough to counteract the losses by ablation (mainly summer) and collapse by calving processes in this glacier.

Acknowledgments

We thank the Peruvian Antarctic Program-Ministry of Foreign Affairs for providing logistical support in the framework of the XXVI (2018–2019) and XXVII (2019–2020) Peruvian Expeditions to Antarctica, and as well as the personnel of the Antarctic Operations Company of the Peruvian Army for the continuous support during our fieldwork. Special thanks to the Editor and anonymous reviewers for their comments, suggestions and corrections that helped to improve the manuscript.

REFERENCES

ALLISON I, FIERZ C, HOCK R, MACKINTOSH A, KASER G & NUSSBAUMER S. 2019. IACS: Past, present, and future of the International Association of Cryospheric Sciences. Hist Geo- Space Sci 10: 97-107.

ARIGONY-NETO J, SAURER H, SIMÕES JC, RAU F, JAÑA R, VOGT S & GOSSMANN H. 2009. Spatial and temporal changes in dry-snow line altitude on the Antarctic Peninsula. Climatic Change 94(1–2): 19-33.

BAMBER J, WESTAWAY R, MARZEION B & WOUTERS B. 2018. The land ice contribution to sea level during the satellite era. Environ Res Lett 3: 1-21.

BELLO C, SUAREZ W & BRONDI F. 2023. Determining the geodetic mass balance of the Znosko glacier (King George Island, Antarctica) using an unmanned aerial vehicle. Remote Sens Lett 14(2): 148-156.

BELLO C, SUAREZ W & LAVADO-CASIMIRO W. 2022. Trends and space-time patterns of near-surface temperatures on Maxwell Bay, King George Island, Antarctica. Int J Climatol 42(14): 7426-7442.

BELLO C, SANTILLAN N, COCHACHIN A, ARIAS S & SUAREZ W. 2020. Ice thickness using ground penetrating radar at Znosko Glacier on King George Island. 2020 IEEE Latin American GRSS & ISPRS Remote Sensing Conference (LAGIRS): 539-541.

BERTHIER E, SCAMBOS TA & SHUMAN CA. 2012. Mass loss of Larsen B tributary glaciers (Antarctic Peninsula) unabated since 2002. Geophys Res Lett 39(13): 1-6.

BIRKENMAJER K. 2002. Retreat of Ecology Glacier, Admiralty Bay, King George Island (South Shetland Islands, West Antarctica) 1956-2001. Bull Polish Acad Sci 50: 15-29.

CARRASCO J. 2013. Decadal changes in the near-surface air temperature in the Western Side of the Antarctic Peninsula. Atmosph Climate Sci 03(03): 275-281.

COGLEY J ET AL. 2011. Glossary of glacier mass balance and related terms (Technical Documents in Hydrology), Paris: UNESCO-IHP, 115 p.

COOK A J, VAUGHAN DG, LUCKMAN A J & MURRAY T. 2014. A new Antarctic Peninsula glacier basin inventory and observed area changes since the 1940s. Antarct Sci 26(6): 614-624.

CUFFEY K & PATERSON WS. 2010. The Physics of Glaciers, 4th ed., Burlington: Butterworth-Heinemann/Elsevier, p. 704.

DA ROSA K, PERONDI C, VEETTIL B, AUGER J & SIMÕES J. 2020. Contrasting responses of land-terminating glaciers to recent climate variations in King George Island, Antarctica. Antarct Sci 32(5): 398-407.

DOBHAL D. 2011. Glacier BT. In: Singh V, Singh P & Haritashya U (Eds), Encyclopedia of Snow, Ice and Glaciers, Dordrecht: Springer Netherlands, p. 376-377.

DYURGEROV M. 2002. Glacier mass balance and regime: data of measurements and analysis, Colorado: 268 p.

FALK U, SILVA-BUSSO A & PÖLCHER P. 2018. A simplified method to estimate the run-off in Periglacial Creeks: A case study of King George Islands, Antarctic Peninsula. Phil Trans R Soc A 376: 20170166.

FERRON F, AQUINO F & SETZER A. 2004. Air temperature time series for King George Island, Antarctica. Pesq Antárt Bras 4: 155-169.

FISCHER A. 2010. Comparison of direct and geodetic mass balances on a multi-annual time scale. Cryosph Discuss 4(3): 1151-1194.

FRANCOU B & POUYAUD B. 2004. Metodos de observacion de glaciares en los Andes tropicales - Mediciones de terreno y procesamientos de datos, La Paz: IRD, 243 p.

HAEBERLI W. 2011. Glacier Mass Balance BT. In: Singh V, Singh P & Haritashya U (Eds), Encyclopedia of Snow, Ice and Glaciers: Springer, Netherlands, p. 399-408.

HAGG W, BRAUN L, UVAROV V & MAKAREVICH, K. 2004. A comparison of three methods of mass-balance determination in the Tuyuksu glacier region, Tien Shan, Central Asia. J Glaciol 50(171): 505-510.

JANSSON P, HOCK R & SCHNEIDER T. 2003. The concept of glacier storage: a review. J Hydrol 282(1-4): 116-129.

JOHNSTON K, VERHOEF J & KRIVORUCHKO K. 2001. Using ArcGIS™ Geostatistical Analyst, New York: ESRI™, 306 p.

KASER G, FOUNTAIN A & JANSSON P. 2003. A manual for monitoring the mass balance of mountain glaciers, Paris: UNESCO (IHP-VI), 137 p.

KEJNA M, ARAŹNY A & SOBOTA I. 2013. Climatic change on King George Island in the years 1948-2011. Pol Polar Res 34(2): 213-235.

LAGGER C, NIME M, TORRE L, SERVETTO N, TATIÁN M & SAHADE R. 2018. Climate change, glacier retreat and a new ice-free island offer new insights on Antarctic benthic responses. Ecography 41: 579-591.

LLIBOUTRY L. 1964. Traité de Glaciologie, 1st ed., Paris: Masson, 428 p.

LLIBOUTRY L. 1974. Multivariate statistical analysis of glacier annual balances. J Glaciol 13 (69): 371-392.

MAVLYUDOV BR. 2014. Ice mass balance of the Bellingshausen ice cap in 2007-2012 (King George Island, South Shetland Islands, Antarctica). Ice and Snow 54(1): 27-34.

MITAS L & MITASOVA H. 2005. Spatial Interpolation BT. In Longley P, Goodchild M, Maguire D & Rhind D (Eds), Geographic Information Systems: Principles, Techniques, Management and Applications, 2ª ed, Vol. 1: John Wiley & Sons, Spain, p. 481-492.

NAVARRO F, JONSELL U, CORCUERA M & MARTÍN-ESPAÑOL A. 2013. Decelerated mass loss of Hurd and Johnsons Glaciers, Livingston Island, Antarctic Peninsula. J Glaciol 213: 115-128.

OLIVA M, NAVARRO F, HRBÁ F, HERNÁNDEZ A, NÝVLT D, PEREIRA P, RUIZ-FERNÁNDEZ J & TRIGO R. 2016. Recent regional climate cooling on the Antarctic Peninsula and associated impacts on the cryosphere. Sci Total Environ 580: 210-223.

OLIVER MA & WEBSTER R. 1990. Kriging: a method of interpolation for geographical information systems. Int J Geogr Inf Syst 4(3): 313-332.

OSTREM G & BRUGMAN M. 1991. Glacier Mass-Balance Measurements. A manual for field and office work. Saskatoon: Environment Canada, 224 p.

OSTREM G & STANLEY A. 1966. Glacier mass balance measurements, a manual for water on the surface of glacier ice. Geografiska field work: Glaciology Section, 81 p.

PATERSON WS. 1994. The Physics of Glacier, 3rd ed., Pergamon, 26-52 p.

PĘTLICKI M, SZIŁO J, MACDONELL S, VIVERO S & BIALIK R. 2017. Recent deceleration of the ice elevation change of Ecology Glacier, King George Island, Antarctica. Remote Sensing 9(6): 18.

RGI CONSORTIUM. 2017. Randolph Glacier Inventory - A Dataset of Global Glacier Outlines: Version 6.0 GLIMS Technical Report RGI. Global Land Ice Measurements from Space, Colorado, USA. Digital Media, 4(July), 71 p.

RIVERA A, BOWN F, NAPOLEONI, F, MUÑOZ C & VUILLE M. 2016. Balance de masa glaciar, Valdivia: CECs, 207 p.

ROTT H, MÜLLER F, NAGLER T & FLORICIOIU D. 2011. The imbalance of glaciers after disintegration of Larsen-B ice shelf, Antarctic Peninsula. Cryosphere 5(1): 125-134.

RÜCKAMP M & BLINDOW N. 2012. King George Island ice cap geometry updated with airborne GPR measurements. Earth Syst Sci Data 4(1): 23-30.

RÜCKAMP M, BLINDOW N, SUCKRO S, BRAUN M & HUMBERT A. 2010. Dynamics of the ice cap on King George Island, antarctica: Field measurements and numerical simulations. Ann Glaciol 51(55): 80-90.

SIBSON R. 1981. A Brief Description of Natural Neighbor Interpolation. In: Barnett V (Ed), Interpolating multivariate data. New York: John Wiley, p. 21-36.

SIEGERT M ET AL. 2019. The Antarctic Peninsula under a 1.5 °C global warming scenario. Front Environ Sci 7: 102.

SILVA A, ARIGONY-NETO J, BRAUN M, ESPINOZA J, COSTI J & JANÃ R. 2020. Spatial and temporal analysis of changes in the glaciers of the Antarctic Peninsula. Global Planet Change 184: 103079-103103.

SIMÕES C, KELLEM K, ROSA D & FERNANDA F. 2015. Collins Glacier retreat process and regional climatic variations, King George Island, Antarctica. Geogr Rev 105: 462-471.

SIMÕES J, BREMER U, AQUINO F & FERRON F. 1999. Morphology and variations of glacial drainage basins in the King George Island ice field, Antarctica. Ann Glaciol 29: 220-224.

SIMÕES J, DAN N, BREMER UF, AQUINO FE & ARIGONY-NETO J. 2004. Small cirque glaciers retreat on Keller Peninsula, Admiralty Bay, King George Island, Antarctica. Pesq Antart Bras 4: 49-56.

SMITH WHF & WESSEL P. 1990. Gridding with continuous curvature splines in tension. Geophysics 55(3): 293-305.

SOBOTA I, KEJNA M & ARAŹNY A. 2015. Short-term mass changes and retreat of the Ecology and Sphinx glacier system, King George Island, Antarctic Peninsula. Antarct Sci 27(5): 500-510.

TURNER J, LU H, WHITE I, KING J, PHILLIPS T, HOSKING J, BRACEGIRDLE T, MARSHALL G, MULVANEY R & DEB P. 2016. Absence of 21st century warming on Antarctic Peninsula consistent with natural variability. Nature 535 (7612): 411-415.

How to cite

SUAREZ W, BELLO C, CRUZ R, ZEGARRA J, ARIAS S & BRONDI F. 2023. Glaciological Mass balance of Znosko Glacier, King George Island. An Acad Bras Cienc 95: e20220821. DOI 10.1590/0001-3765202320220821.

Manuscript received on September 21, 2022;
accepted for publication on October 13, 2022

WILSON SUAREZ[1,2]
https://orcid.org/0000-0002-3409-790X

CINTHYA BELLO[3]
https://orcid.org/0000-0003-4154-6379

ROLANDO CRUZ[4]
https://orcid.org/0000-0001-7166-3053

JUAN ZEGARRA[4]
https://orcid.org/0000-0002-4984-1738

SANDRO ARIAS[1]
https://orcid.org/0000-0002-8747-4895

FABIAN BRONDI[5]
https://orcid.org/0000-0002-1582-4892

[1]National Service of Meteorology and Hydrology of Peru/SENAMHI, St. Cahuide 785, Jesús María, Lima, Perú

[2]National Agrarian University La Molina/UNALM, Doctorate in Water Resources/DRH, Av. La Molina s/n, La Molina, Lima, Perú

[3]Universidad Científica del Sur, Carrera de Biología Marina, Panamericana Sur km 19, Villa El Salvador 15067, Perú

[4]National Water Authority/ANA, St. Los Petirrojos 355, San Isidro, Lima, Perú

[5]National Geographic Institute of Peru/IGN, Av. Andrés Aramburu 1184, Surquillo, Lima, Perú

Correspondence to: **Wilson Suarez Alayza**
E-mail: wsuarez@senamhi.gob.pe